Journal of Photonics for Energy 9.3 (2019): 034001

DOI: https://doi.org/10.1117/1.JPE.9.034001

Microwave plasma and rapid thermal processing of Indium-Tin oxide thin films for enhancing their performance as transparent electrodes

R. Ramadan[1,2,*], K. Abdelhady[2], M. Manso-Silván[1], V. Torres-Costa[1], and R.J. Martín-Palma[1]

[1]Departamento de Física Aplicada, Universidad Autónoma de Madrid, 28049 Madrid, Spain.

[2]Physics Department, Faculty of Science, Minia University, Minia, 61519, Egypt.

* Corresponding author: E-mail address: rehab.ramadan@predoc.uam.es

ABSTRACT

Indium-tin oxide (ITO) is widely used as a transparent electrode for optoelectronic devices given its large transparency and high conductivity. However, the particular properties of this material greatly depend on the overall fabrication process. In this work, we report on the effect of four different post-fabrication processes on ITO thin films grown by electron beam evaporation. More specifically, the effect on the overall properties of evaporated ITO thin films of microwave plasma annealing, rapid thermal processing, and the two processes combined were analyzed. In particular, the morphological, chemical, optical, and electrical properties of the annealed ITO thin films were studied and discussed. The experimental results show that the ITO thin films can be turned from opaque to transparent and their conductivity can be improved by one order of magnitude depending on the particular post-fabrication process.

Keywords: Indium- tin oxide, microwave plasma annealing, rapid thermal processing, surface morphology and optoelectronic properties.

1. INTRODUCTION

Transparent conductive oxides (TCOs) have large band gaps while their Fermi level is located in the conduction band due to free-carrier producing centers [1]. These properties make TCOs very good candidates for their use as transparent electrodes in the development of photonic and optoelectronic devices. In particular, TCOs have been used for the fabrication of organic light-emitting (OLED) devices [2], liquid crystal displays [3], electrochromic windows [4], and photovoltaic solar cells [5]. Logically, their optimum performance relies on a large optical transparency in the visible range combined with high electrical conductivity. However, although TCOs have been used for several applications during the past six decades, many unanswered questions at both the fundamental and applied levels still remain.

TCOs can be made out of p-type and n-type semiconductor materials. p-type TCOs, such as cupric oxide, have found very limited applications since the fabrication of efficient p-type TCOs remains an outstanding challenge. For instance, they have been used in bi-facial and multijunction cells [6]. Accordingly, most commercially available TCOs are n-type semiconductor materials, including Sn-doped In_2O_3 (ITO) [7], Al-doped ZnO [8], and F-doped SnO_2 [9]. Among these, ITO has the best optoelectronic properties because it has high electrical conductivity and large transparency in the visible region of the spectrum, together with high reflectance in the infrared wavelength interval. Besides, this material has a wide bandgap (E_g = 3.5 − 4.2 eV) [10], [11].

There are many different techniques used for the deposition of ITO thin films, although most of them are based on vacuum processes such as DC magnetron sputtering [12, 13], RF magnetron sputtering [14], chemical vapor deposition [15], pulsed laser deposition [16], reactive ion plating [17], and electron beam evaporation [18]. Electron beam (e-beam) evaporation is one of the most effective techniques used for the deposition of ITO thin films with high electrical conductivity and large optical transparency. However, there are many parameters which affect the overall quality of the evaporated thin films. These include doping level, annealing process, and the factors related to the specific method of evaporation. For example, the properties of thin films grown by e-beam evaporation are affected by such parameters as the pressure in the vacuum chamber, electron beam

intensity, evaporation rate, etc. All these experimental variables have a notable effect on the chemical composition, crystallinity, electrical conductivity, and optical properties of the TCOs [18].

In this work, we present our findings regarding the study of the effect of four different annealing processes on ITO thin films grown by electron beam evaporation. More specifically, the effect of microwave plasma annealing (MwPA), rapid thermal annealing, and these two processed combined on the overall properties of evaporated ITO thin films is analyzed. In particular, the morphological, chemical, optical, and electrical properties of the resulting ITO thin films are studied in detail. We aim at understanding the particular mechanisms responsible for the unique combination of optical and electrical transport properties of the fabricated ITO thin films.

2. EXPERIMENTAL

2.1 Fabrication and processing techniques

Indium tin oxide (ITO) thin films were evaporated on quartz and silicon substrates (1.5×1.5 cm^2) by electron beam (e-beam) evaporation. The source material is indium oxide/tin oxide, 90%/10%wt.%, which was purchased from the Kurt J. Lesker Company. The typical base pressure was 2×10^{-7} Torr, which grew to $4-6\times10^{-5}$ Torr during the evaporation process. The evaporation process was carried out without introducing any reactive gases. The substrate was located at around 30 cm over the ITO target. The emission current was 30 mA and the deposition time was 30 minutes. It is worth noticing that the thin films showed a brownish tonality upon evaporation.

Rapid thermal processing (RTP) in oxygen atmosphere at 550 ºC for 5 minutes was used to change the overall properties of the thin films. The heating ramp until the desired temperature was reached was of around 52.5ºC/s and the cooling ramp was around 17.5ºC/s. It was observed that the thin films subjected to RTP treatments showed large transparency.

In addition to RTP, the effect of microwave plasma annealing (MwPA) on the ITO thin films grown by evaporation was studied. The MwPA system consists of a cylindrical glass

vacuum chamber inserted in a stainless steel earthed hood. An open window orients the Mw wave-guide to the glass cylinder, while the hood acts as a resonant cavity for the solid state generated microwaves (2.45 MHz, up to 600 W). The conditions of the atmosphere are controlled through an exhaust valve with a rotary pump allowing a background pressure of 2×10^{-2} mbar and a common inlet for reactive and inert gasses with individual gas flow meters. A grounded, refrigerated stainless steel substrate holder exposes the sample horizontally to the Mw plasma. MwPA treatments were performed in an argon atmosphere, with a typical pressure of 0.1 mbar for 2 minutes ON/OFF steps every 60 s and at a maximum power of 600W [19].

2.2 Characterization techniques

The morphology of the thin films was studied by field emission scanning electron microscopy (FESEM) using a Philips XL- 40FEG microscope operated at 10 kV. An Energy Dispersive Spectroscopy X-ray analyzer (EDX, Inca X-sight 7558, Oxford Instruments) coupled to the microscope was used to determine the elemental compositions of the films.

X-ray diffraction (XRD) studies were performed using a Siemens D5000 HR diffractometer in the grazing-incidence configuration using Cu-Kα radiation (λ=1.54 Å), a fixed incidence angle of 0.5 degrees and 2θ range from 20^0 to 70^0 with 0.04^0 increments and 10 s accumulation time.

Optical characterization in the UV-visible range (300-850 nm) of the ITO thin films, comprising transmittance (T) and reflectance (R), was carried out using a Jasco V-560 double-beam spectrophotometer, equipped with an integrating sphere to avoid scattering losses. For this particular purpose, the ITO thin films were deposited on quartz substrates. The spectral values of the optical constants (index of refraction, n, and extinction coefficient, k) and the thin film thickness were determined using a program developed in our laboratories based on genetic algorithms [20].

The resistance of the thin films was measured using the two point probe method. A homemade cell consisting of two movable copper probes (with a diameter of 0.5 mm) and

a grounded copper base (2×2 cm^2). The distance between the two probes was 1.5 cm. The measurements were carried out in a Faraday's box to shield them from external signals. The electrical measurements were carried out in a Bio- Logic SP-150 potentiostat with a scan rate 20 mV/s and applied potential in the 0 to 1 V range.

All the measurements were performed on samples grown onto monocrystalline Si substrates except the optical measurements for which quartz substrates were used.

3. EXPERIMENTAL RESULTS

Five different sets of ITO thin films were the subject of the present study, namely (1) as-deposited thin films and thin films subjected to (2) MwPA, (3) RTP, (4) MwPA plus subsequent RTP (MwPA+RTP), and (5) RTP plus subsequent MwPA (RTP+MwPA). The morphological, chemical, structural, optical, and electrical properties of the previously described sets of thin films were studied. The results are described in the following sections.

3.1 Morphology

Fig. 1 shows typical cross-sectional FESEM images of the different ITO thin films before and after processing. It is evident that, in all cases, the ITO thin films show good homogeneity, both from the point of view of the overall structure and thickness. Besides, no cracks or other imperfections are manifested. Moreover, it is observed that the ITO thin films show a granular composition. What is more, the different images show clear differences in the average sizes of the nanoparticles which compose the thin films, an effect which most likely has its origin in the different annealing processes. As we will see below, MwPA processing has a notable effect on the crystallinity of the thin film, since MwPA-processed samples present the largest particle size as determined by XRD analysis. This issue will be discussed in detail in the next section.

From the cross-sectional FESEM images, the thickness of the various thin films was determined by means of the image analysis program package Imagej [21]. The values are presented in Table 1, from which it is observed that the thickness slightly decreases upon annealing [10], probably due to film compaction by heat treatment. This effect might have

its origin in partial crystallization as will be discussed in section 3.3 (Structural properties).

Table 1: Thickness of the ITO thin films before and after the different post-deposition treatments, experimental values of the sheet resistance, resistivity, and *2θ (°)* for the *(222)* plane. FWHM and grain size (*D*) of the ITO thin films determined from the XRD spectra.

ITO thin film name	Film Thickness (nm)	Sheet resistance (Ω/□)	Resistivity×10^{-4} ± 0.5 (Ω.cm)	*2θ (°)* for the plane *(222)*	FWHM (radian)	Grain size (nm)
As deposited	574	84.98	48.7	32.20	3.84	2.16
MwPA	570	3.51	2.0	30.72	0.4527	18.33
RTP	566	29.24	16.5	30.70	0.4847	17.12
MwPA+RTP	540	28.02	15.1	30.75	0.5070	16.36
RTP+MwPA	518	8.30	4.3	30.73	0.5359	15.48

3.2 Semi-quantitative EDX microanalysis

Fig. 2 gives the elemental compositions of the different ITO thin films deposited on Si (100) substrates. The experimental results confirm that, as expected, In, Sn and O are the main elements of the ITO thin films. It has to be noted that the Si signal comes from the substrate and the small Cr signal has its origin in the very thin layer (around 15 nm) deposited by sputtering before FESEM characterization for metallization. The images prove that all the films are free from contaminants and show a quite good compositional homogeneity. Fig. 2(6) depicts the weight percentage of In and Sn in the different ITO films, from which a slight variation of the relative content of the two elements is noted. This indicates that the post-formation processes (RTP, MwPA, and their combination) do not have a notable effect on the main elemental compositions. These results agree with previous studies [22], [23]. Furthermore, the Sn to In ratio remains almost constant and close to the doping concentration value of Sn in the source material, which is indium oxide/tin oxide: 90%/10%wt.%.

3.3 Structural properties

The microstructure of the ITO thin films was studied by X-Ray Diffraction (XRD) analysis. It is well known that the microstructure of the ITO thin films is extremely sensitive to the specific annealing process, as previously reported [10]. Our experimental results, shown in Fig. 3, allow to conclude that the as-deposited ITO thin films are amorphous and only one single broad diffraction peak is observed. However, all processed thin films show a well-defined crystalline structure with diffraction peaks corresponding to specific crystallographic planes. In particular, the (222) plane appears as the preferred orientation as demonstrated by the highest intensity of the corresponding diffraction peaks. This observation is in agreement with previous works [10], [24]. Additionally, it is noted that annealing of ITO thin films has a notable effect on the grain size (D).

In order to estimate the grain size of the ITO thin films from the preferential oriented (hkl) crystal plane, the Debye Scherrer formula [25] was used:

$$D = \frac{0.94\,\lambda}{\beta\,\cos\theta},$$

where λ is the wavelength of the X-ray radiation used (λ=0.154 nm in our case), β is the measured broadening of the diffraction line at half maximum intensity (FWHM) in radians, and θ is the corresponding Bragg's diffraction angle of the main peak in the XRD plots. For the experimental determination of the values of D, the (222) plane was used given these show the largest intensity, as pointed out before. The experimental results, which are summarized in Table 1, indicate that the grain sizes for all the processed samples are larger than those of the as-deposited film. Besides, thin films processed by MwPA show the largest values, which was previously ascertained by FESEM analysis (Section 3.1). However, it has to be noted that the XRD peaks can be widened by defects and internal stress. For this reason, the mean values of D calculated by this method are generally smaller than the real ones [26].

3.4 Optical properties

Fig. 4 shows typical reflectance (R) and transmittance (T) spectra of as-deposited ITO thin films grown on quartz substrates. It is observed that T is negligible, while the

reflectance spectrum is practically flat and the values are around 20 % in the 400-850 nm wavelength range. However, MwPA processing of the ITO thin films leads to notable changes in the optical properties, i.e., while *T* remains close to zero, the values of reflectance are quite low at short wavelengths but increase towards the infrared, as depicted in Fig. 4. Fig. 5 portrays the *R* and *T* spectra of the ITO thin films upon RTP processing, and a combination of the two previous techniques, namely MwPA+RTP and RTP+MwPA. The experimental spectra confirm the high transparency of the three different thin films, with an average value of *T* around 85% and of *R* about 12. Additionally, it is observed that the experimental curves present a few maxima and minima in the visible and near infrared wavelength regimes, due to interference effects. The position of the maxima and minima remains almost constant for the three samples, which confirms the small variation of the thickness of the thin films after the annealing processes and also the minor variation of the chemical composition, leading to small variations of the index of refraction. This particular issue will be discussed later in this section. Finally, below about 400 nm a quite large absorption is clearly observed, not attributable to the substrate, since quartz substrates were used for the optical measurements.

From the experimental optical *T* and *R* spectra of the ITO thin films, the values of the optical constants, refractive index (*n*) and extinction coefficient (*k*), were extracted. For this purpose, a program developed in our laboratories was used [20]. Figs. 6 and 7 show the spectral values of *n* and *k*, respectively, for the ITO thin films. The results show that the values of *n* decrease with increasing wavelength for all the ITO thin films. Moreover, the experimental results show that annealing leads to increased values of the index of refraction for all the treated thin films. This effect is attributed to the crystalline structure of the ITO thin films upon processing, as determined by XRD analysis (Section 3.3). As previously indicated, the grain size increased from around 2 nm for as-deposited thin films to about 16 nm for the annealed ITO thin films. As a result of the crystallinity of the processed thin films, the ITO nanocrystals are more closely packed together. As such, the thin films are more compact leading to a higher refractive index as a consequence of the reduction of void space. These results are in agreement with previous works, such as those which studied the effect of Sn doping on the properties of ITO thin films prepared by e-beam evaporator [27], the effect of annealing processes on the optical constants of MgF_2 thin films [28], TiO_2 nanostructured thin films [29], and annealed $Cd_{1-x}Zn_xSe$ thin

256 films (with $x = 0$, 0.40 and 1) [30]. Wherefore, the curves for the transparent films (RTP,
257 MwPA+RTP, and RTP+MwPA) show a small variation in the spectral values of n and
258 this limited variation agrees with the rather small changes in the thickness, grain size, and
259 transparency. A similar behavior for the spectral values of the extinction coefficient is
260 observed, as depicted in Fig. 7. The values of k are very small and close to zero for all the
261 samples as a consequence of the small optical absorption of the ITO films, leading to
262 large transparency in the visible range. More specifically, the three transparent thin films,
263 RTP, MwPA+RTP, and RTP+MwPA, show very low values of k, below 10^{-3}. However,
264 the opaque thin films, namely as-deposited ITO and MwPA-processed, have values of k
265 larger than 10^{-1}, as shown in Fig. 7.

266 In addition, the values of the optical band gap for the transparent ITO thin films, i.e., thin
267 films treated by RTP, MwPA+RTP and RTP+MwPA, were extracted by using Tauc plots
268 [31], as shown in Fig. 8. The absorption coefficient (α) of the films were determined from
269 optical measurements in the 400 to 850 nm wavelength range. Afterwards, the
270 relationship between $(\alpha.d)^2$ and the photon energy was plotted, assuming that ITO thin
271 films show a direct band gap character [32]. The band gap can be calculated by
272 extrapolating the straight line of the relation between $(\alpha.d)^2$ and photon energy ($h\upsilon$). The
273 results, portrayed in Fig. 8, show that the change in the energy gap for the ITO thin films
274 is quite small which is in agreement with the overall optical behavior of the three films
275 discussed above. Accordingly, it can be concluded that MwPA combined with RTP does
276 not have a noticeable effect on the optical properties of the ITO thin films, as a
277 consequence of small variations of the index of refraction, having its origin in limited
278 variations of the chemical properties of the thin films. A similar behavior has been
279 previously reported (see, for instance, references [10], [33].

280

281 **3.5 Electrical properties**

282

283 The electrical behavior of the ITO thin films was determined using the two-point probe
284 method [34]. From the electrical (current-voltage) measurements a linear relationship is
285 found in all cases, as portrayed in Fig. 9, leading to an ohmic electrical behavior.
286 Accordingly, the experimental data were fitted to a linear regression, from which the
287 values of the resistance of every ITO thin film were extracted using Ohm's law [35]. The

experimental results show that the annealing process has a notable effect on the resistivity of the ITO thin films, as shown in Table 1. In particular, MwPA processing at 0.1 mbar for 2 minutes cause a remarkable reduction in the resistivity of the ITO thin films, although from an optical point of view the thin film remains opaque. However, applying RTP in oxygen atmosphere at 550ºC results in thin films with a large degree of transparency (Fig. 5) and good conductivity. This is probably due to the increased crystalline structure created by the annealing process, as determined by XRD analysis (sec. 3.3), given that grain boundaries in polycrystalline and amorphous materials tend to decrease the electrical conductivity of any given material [36]. In fact, grain boundaries are considered two-dimensional defects in the crystal structure. From Table 1, it is worth mentioning that microwave processing has a very large impact on lowering the resistivity of the deposited films. However, as determined in the previous section, the thin films are still opaque. As such, we resorted to using both methods combined together, i.e., MwPA+RTP and RTP+MwPA. As a result of the combined post-formation processes, the ITO thin films show a quite large optical transparency and high conductivity. However the best results are obtained for the films treated by RTP first which has a resistivity equal 4.3×10^{-4} Ω.cm as indicated in Table 1. Table 2 presents a comparison between the previously reported electrical and optical properties of ITO thin films prepared by different methods and for the best combined process of the present work. According to Table 2, the optical and electrical properties for (MwPA+RTP) sample is better than the previously obtained results by e-beam evaporation due to the combination of the thermal processing with MwPA.

Table 2: Summary of the optical and electrical properties of ITO thin films previously manufactured by different techniques compared with the best results obtained in this work.

Manufacturing Technique	Average transmission (λ= 300-800 nm)	Resistivity× 10^{-4} (Ω.cm)	Reference
RF magnetron sputtering	87.5	5.3	[11]
DC Magnetron Sputtering	79	5	[13]
Reactive low voltage ion plating	84	4	[17]
e-beam evaporator	75	5.8	[18]
RF magnetron sputtering	88	< 10	[32]
e-beam evaporator	85	4.3	Present work

4. DISCUSSION

Table 3 provides a summary of the key properties of the ITO thin films before and after being subjected to the different post-formation treatments. The experimental results indicate that the as-deposited and MwPA ITO thin films are opaque, while the rest of the thin films (processed by RTP, MwPA+RTP, and RTP+MwPA) are transparent. Additionally, the MwPA ITO thin films show the highest conductivity.

Table 3: Summary of the optical, structural, and electrical properties of the ITO thin films.

ITO thin films	Optical properties					Crystal structure	Resistivity $\pm 0.5\times10^{-4}$ (Ω.cm)
	T%	R%	(n)	(k)	(α)		
As deposited	Opaque thin films	The highest R% average over all the wavelength range	Annealing process causes an increase of (n) for all the treated thin films	Annealing process causes a decrease of (k) for all the treated thin films	High for the opaque films	Amorphous with one broad peak	48.7
MwPA		Low R% at shorter wavelengths, but increases toward the infrared region				Crystalline and the preferential oriented crystal plane is (222)	2.0
							16.5
RTP	Highly Transparent Thin films	Low R% average over all the wavelength range			Low for the transparent films		
MwPA+RTP							15.1
RTP+MwPA							4.3

In particular, the as-deposited ITO thin films are opaque and their electrical conduction properties are inferior to those of the processed thin films. The higher resistivity of ITO films is generally attributed to the low carrier concentration, which is directly related to the oxygen content [37]. This way, an oxygen vacancy gives rise to shallow donor states just below the conduction band by releasing two electrons. Also, one-electron or impurity states are formed below the In 5s or 5p conduction band by substitution of In^{3+} by Sn^{4+}. The improvement in the degree of crystallinity causes an increase in the concentration of electrically active sites, which would increase the carrier concentration [38], [39].

Microwave energy generates thermal heating associated with atomic vibration and/or dipole rotation in the thin films [40]. This technique has unique features, including volumetric heating, i.e., the capability of transferring energy directly to the interior of the thin film enabling the annealing process to be carried out at low temperature rapidly, and short processing times [41]. Microwave annealing processes were used before as dopant activation in silicon and for the recrystallization of amorphous silicon films [42]. As indicated in Table 3, the MwPA-treated ITO thin films are opaque and their electrical

conduction properties are very good. The experimental results show that microwave processing does not change the opaque nature of the as-deposited ITO thin films, probably because oxygen deficiencies still remain. It must be here remembered that microwave processing is carried out in argon. As such, from the optical point of view, the MwPA-processed films show large absorption coefficients. However, the ITO thin films become more conductive. We attribute this increase in the electrical conductivity to the doped tin atoms. The activated dopants, Sn^{+4} ions in our case, would be responsible for substituting In^{+3} to form donor levels in the energy band gap, which leads to an increase in the number of charge carriers. The interaction between the argon gas atoms and the ITO thin film atoms increase the atomic vibrations and, as a result, more ionized Sn^{+4} ions are activated and the generated film transferred from the amorphous state to be crystalline with larger grain size (as determined by FESEM and XRD analysis) than the as-deposited films.

From Table 3 it is observed that RTP-processed ITO thin films are transparent and good conductors. Moreover, the electrical properties of RTP and (MwPA+RTP)-processed ITO thin films are comparable, although quite different from those of (RTP+MwPA)-processed thin films. In our opinion, thermal annealing under oxygen atmosphere gradually re-oxidizes the In and Sn particles and oxygen vacancies are thus formed again, which increases the conductivity of the thin films. Besides, the degree of crystallinity of the ITO thin films increases with particles of large grain size. The previously mentioned effects also contribute to the larger transparency of the thin films, with low absorption coefficients.

Combining the two post-formation processes, i.e., RTP and MwPA, results in transparent and low-resistivity thin films due to oxygen vacancies generated by the thermal annealing process in oxygen. (RTP+MwPA)-processed thin films show higher conductivity than (MwPA+RTP)-processed thin films. This behavior might occur because microwave annealing after rapid thermal processing activates more Sn^{+4} ions due to atomic vibrations. In this case, Sn^{+4} ions would substitute In^{+3} to form donor levels in the band gap, thus leading to an increased number of charge carriers as discussed before. However, oxygen vacancies would not be affected by microwave annealing, so the ITO thin film would preserve its large transparency, as indicated in the optical properties section.

Finally, it is worth pointing out that the (MwPA+RTP)-processed thin films have almost the same optical and electrical properties as RTP-processed thin films, although showing lower conductivity than (RTP+MwPA)-processed thin films. We hypothesize that rapid thermal processing after microwave annealing results in the oxidation of Sn and In metal particles. Accordingly, the observed decrease in conductivity would be of the same order of magnitude as that of RTP-treated thin films. In the three cases, the crystalline structure would not be affected.

5. CONCLUSIONS

The effect of four different annealing processes on the morphological, chemical, optical, and electrical properties of ITO thin films grown by electron beam evaporation has been analyzed in this work.

From the point of view of their morphology, it was found that MwPA processing results in increased the grain size from 2 nm for as deposited ITO thin films to around 18 nm while, at the same time, the electrical resistivity decreases from 48.7×10^{-4} to 2.0×10^{-4} Ω.cm. However, the thin films are still opaque due to oxygen deficiency. Furthermore, it was found that combining MwPA with RTP leads to a notable improvement in the optical transparency of the ITO thin films in addition to their crystalline structure and a good electrical conductivity (in the order of 10^3 $S.cm^{-1}$). Additionally, it was determined that the chemical composition of the ITO thin films is slightly affected by the different post-formation treatments (MwPA, RTP, and the two processes combined). Besides, ITO thin films treated by MwPA after RTP show the highest conductivity with very good degree of transparency, which makes this process the most appropriate for the fabrication of ITO thin films for applications in optoelectronics as transparent electrodes, including electroluminescent devices, flat panel displays, and solar cells.

ACKNOWLEDGEMENTS

This work was partially supported by the Egyptian ministry of higher education missions section under Egyptian joint supervision Grant at UAM Spain for PhD degree. We would

like to thank the Egyptian institute, cultural office of the Egyptian embassy in Madrid, Spain. The authors are thankful to Mr. Luis García Pelayo for technical support.

6. REFERENCES

[[1] S. Lany, A. Zunger, Dopability, intrinsic conductivity, and nonstoichiometry of transparent conducting oxides, Physical Review Letters, 98 (2007) 045501.
[2] P. Bettotti, Hybrid materials for integrated photonics, Advances in Optics, 2014 (2014).
[3] P. Krištofová, E. Rudnik, A. Miškufová, Hydrometallurgical methods of indium recovery from obsolete LCD and LED panels, Metallurgy and Foundry Engineering, 42 (2017) 157-170.
[4] M. Kanao, M. Higuchi, Synthesis of Metallo-Supramolecular Polymers with Bis-NNN-Tridentate Ligand for Electrochromic Devices, Journal of Photopolymer Science and Technology, 28 (2015) 363-368.
[5] H. Park, J.A. Rowehl, K.K. Kim, V. Bulovic, J. Kong, Doped graphene electrodes for organic solar cells, Nanotechnology, 21 (2010) 505204.
[6] K. Fleischer, E. Norton, D. Mullarkey, D. Caffrey, I.V. Shvets, Quantifying the Performance of P-Type Transparent Conducting Oxides by Experimental Methods, Materials, 10 (2017) 1019.
[7] M.-s. Hwang, B.-y. Jeong, J. Moon, S.-K. Chun, J. Kim, Inkjet-printing of indium tin oxide (ITO) films for transparent conducting electrodes, Materials Science and Engineering: B, 176 (2011) 1128-1131.
[8] A.C. Aragonès, A. Palacios-Padrós, F. Caballero-Briones, F. Sanz, Study and improvement of aluminium doped ZnO thin films: Limits and advantages, Electrochimica Acta, 109 (2013) 117-124.
[9] J.T. Wang, X.L. Shi, W.W. Liu, X.H. Zhong, J.N. Wang, L. Pyrah, K.D. Sanderson, P.M. Ramsey, M. Hirata, K. Tsuri, Influence of preferred orientation on the electrical conductivity of fluorine-doped tin oxide films, Scientific reports, 4 (2014) 3679.
[10] H. Kim, J. Horwitz, G. Kushto, A. Pique, Z. Kafafi, C. Gilmore, D. Chrisey, Effect of film thickness on the properties of indium tin oxide thin films, Journal of Applied Physics, 88 (2000) 6021-6025.
[11] J.W. Shin, W.J. Cho, Microwave Annealing Effects of Indium-Tin-Oxide Thin Films: Comparison with Conventional Annealing Methods, physica status solidi (a), DOI (2018) 1700975.
[12] H. Askari, H. Fallah, M. Askari, M.C. Mohmmadieyh, Electrical and optical properties of ITO thin films prepared by DC magnetron sputtering for low-emitting coatings, arXiv preprint arXiv:1409.5293, DOI (2014).
[13] M.-J. Keum, J.-G. Han, Preparation of ITO thin film by using DC magnetron sputtering, Journal of Korean Physical Society, 53 (2008) 1580.
[14] R. Bingyan, L. Xiaoping, W. Minhua, X. Ying, Preparation and characteristics of indium tin oxide (ITO) thin films at low temperature by rf magnetron sputtering, Rare Metals, 25 (2006) 137-140.
[15] Y. Zhang, L. Zhang, C. Zhou, Review of chemical vapor deposition of graphene and related applications, Accounts of chemical research, 46 (2013) 2329-2339.
[16] S.L. Ou, D.S. Wuu, S.P. Liu, Y.C. Fu, S.C. Huang, R.H. Horng, Pulsed laser deposition of ITO/AZO transparent contact layers for GaN LED applications, Optics express, 19 (2011) 16244-16251.
[17] D. Huber, H. Pulker, ITO-coatings by reactive low-voltage ion plating: film properties and plasma analysis, Vakuum in Forschung und Praxis, 21 (2009) 29-34.

[18] M. Yamaguchi, A. Ide-Ektessabi, H. Nomura, N. Yasui, Characteristics of indium tin oxide thin films prepared using electron beam evaporation, Thin solid films, 447 (2004) 115-118.
[19] R. Ramadan, J.G. Simiz, M.D. Ynsa, M.M. Silván, Microwave plasma annealing of sol-gel deposited tantalum oxide and zinc oxide films, Vacuum, 149 (2018) 336-342.
[20] V. Torres-Costa, R. Martín-Palma, J. Martínez-Duart, Optical constants of porous silicon films and multilayers determined by genetic algorithms, Journal of applied physics, 96 (2004) 4197-4203.
[21] M.D. Abràmoff, P.J. Magalhães, S.J. Ram, Image processing with ImageJ, Biophotonics international, 11 (2004) 36-42.
[22] A.B. Yadav, A. Pandey, S. Jit, Effects of Annealing Temperature on the Structural, Optical, and Electrical Properties of ZnO Thin Films Grown on n-Si< 100> Substrates by the Sol–Gel Spin Coating Method, Acta Metallurgica Sinica (English Letters), 27 (2014) 682-688.
[23] J. Venkatesan, S.K. Kim, Effect of temperature on isolation and characterization of hydroxyapatite from tuna (Thunnus obesus) bone, Materials, 3 (2010) 4761-4772.
[24] M. Fang, A. Aristov, K.V. Rao, A.V. Kabashin, L. Belova, Particle-free inkjet printing of nanostructured porous indium tin oxide thin films, RSC Advances, 3 (2013) 19501-19507.
[25] A. Patterson, The Scherrer formula for X-ray particle size determination, Physical review, 56 (1939) 978.
[26] A. Ashour, M. Kaid, N. El-Sayed, A. Ibrahim, Physical properties of ZnO thin films deposited by spray pyrolysis technique, Applied Surface Science, 252 (2006) 7844-7848.
[27] V. Senthilkumar, P. Vickraman, M. Jayachandran, C. Sanjeeviraja, Structural and optical properties of indium tin oxide (ITO) thin films with different compositions prepared by electron beam evaporation, Vacuum, 84 (2010) 864-869.
[28] T.-T. Tan, B.-J. Liu, Z.-H. Wu, Z.-T. Liu, Annealing Effects on Structural, Optical Properties and Laser-Induced Damage Threshold of MgF 2 Thin Films, Acta Metallurgica Sinica (English Letters), 30 (2017) 73-78.
[29] P.B. Nair, V. Justinvictor, G.P. Daniel, K. Joy, K.J. Raju, D.D. Kumar, P. Thomas, Optical parameters induced by phase transformation in RF magnetron sputtered TiO2 nanostructured thin films, Progress in Natural Science: Materials International, 24 (2014) 218-225.
[30] I. Ali, A. Iqbal, A. Mahmood, A. Shah, M. Zakria, A. Ali, Optical spectroscopic analysis of annealed Cd1− xZnxSe thin films deposited by close space sublimation technique, Materials Science-Poland, 34 (2016) 828-833.
[31] J. Tauc, Optical properties and electronic structure of amorphous Ge and Si, Materials Research Bulletin, 3 (1968) 37-46.
[32] L. Karmakar, D. Das, Melting point of Sn as the optimal growth temperature in realizing the favored transparent conducting properties of In2O3: Sn films, Journal of Alloys and Compounds, 767 (2018) 642-650.
[33] S.-M. Kim, H.-W. Choi, K.-H. Kim, S.-J. Park, H.-H. Yoon, Preparation of ITO and IZO thin films by using the facing targets sputtering (FTS) method, J. Korean Phys. Soc, 55 (2009) 1996-2001.
[34] S. Beesabathuni, J. Stockham, J. Kim, H. Lee, J. Chung, A. Shen, Fabrication of conducting polyaniline microspheres using droplet microfluidics, RSC Advances, 3 (2013) 24423-24429.
[35] J. Frenkel, On the electrical resistance of contacts between solid conductors, Physical Review, 36 (1930) 1604.
[36] D. Raoufi, A. Taherniya, The effect of substrate temperature on the microstructural, electrical and optical properties of Sn-doped indium oxide thin films, The European Physical Journal Applied Physics, 70 (2015) 30302.
[37] H. Han, D. Adams, J. Mayer, T. Alford, Characterization of the physical and electrical properties of indium tin oxide on polyethylene napthalate, Journal of Applied Physics, 98 (2005) 083705.

[38] M. Albrecht, R. Schewski, K. Irmscher, Z. Galazka, T. Markurt, M. Naumann, T. Schulz, R. Uecker, R. Fornari, S. Meuret, Coloration and oxygen vacancies in wide band gap oxide semiconductors: Absorption at metallic nanoparticles induced by vacancy clustering—A case study on indium oxide, Journal of Applied Physics, 115 (2014) 053504.
[39] Y.S. Jung, J.Y. Seo, D.W. Lee, D.Y. Jeon, Influence of DC magnetron sputtering parameters on the properties of amorphous indium zinc oxide thin film, Thin Solid Films, 445 (2003) 63-71.
[40] Y.-J. Lee, T.-C. Cho, S.-S. Chuang, F.-K. Hsueh, Y.-L. Lu, P.-J. Sung, H.-C. Chen, M.I. Current, T.-Y. Tseng, T.-S. Chao, Low-temperature microwave annealing processes for future IC fabrication—A review, IEEE Transactions on electron devices, 61 (2014) 651-665.
[41] K. Song, C.Y. Koo, T. Jun, D. Lee, Y. Jeong, J. Moon, Low-temperature soluble InZnO thin film transistors by microwave annealing, Journal of Crystal Growth, 326 (2011) 23-27.
[42] C. Fu, Y. Wang, P. Xu, L. Yue, F. Sun, D.W. Zhang, S.-L. Zhang, J. Luo, C. Zhao, D. Wu, Understanding the microwave annealing of silicon, AIP Advances, 7 (2017) 035214.

7. FIGURES CAPTIONS

Figure 1: Cross section FESEM images of the different ITO films: (1) as-formed, (2) MwPA, (3) RTP, (4) MwPA+RTP and (5) RTP+MwPA processed thin films.

Figure 2: EDX analysis of the ITO thin films: (1) as-formed, (2) MwPA, (3) RTP, (4) MwPA+RTP, (5) RTP+MwPA processed thin films and (6) variation of the wt.% of the main elements (In and Sn).

Figure 3: XRD patterns for as-deposited and annealed ITO thin films. The Miller indices of the different planes are indicated.

Figure 4: Transmittance and reflectance spectra of the as-deposited ITO thin film and upon MwPA processing. Note: both *T* spectra are superposed.

Figure 5: Transmittance and reflectance spectra of the ITO thin films after RTP, MwPA+RTP and RTP+MwPA processing.

Figure 6: Variation of the refractive index with wavelength for the as-deposited and processed ITO thin films.

Figure 7: Variation of the extinction coefficient (*k*) with wavelength for the as-deposited and processed ITO thin films.

Figure 8: Tauc's plots used to estimate the values of the energy gap of the transparent thin films.

Figure 9: Current-voltage (*I-V*) curve of the different ITO films with different treatments.

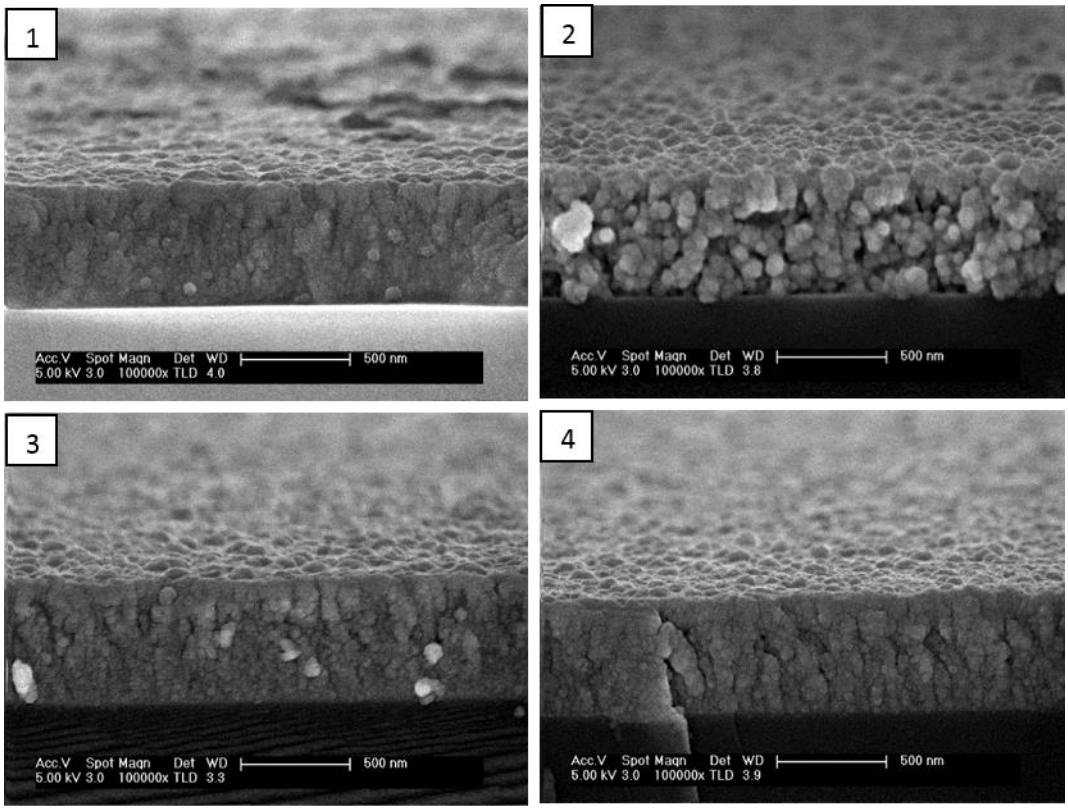
1
Acc.V Spot Magn Det WD 500 nm
5.00 kV 3.0 100000x TLD 4.0
2
Acc.V Spot Magn Det WD 500 nm
5.00 kV 3.0 100000x TLD 3.8
3
Acc.V Spot Magn Det WD 500 nm
5.00 kV 3.0 100000x TLD 3.3
4
Acc.V Spot Magn Det WD 500 nm
5.00 kV 3.0 100000x TLD 3.9
5
Acc.V Spot Magn Det WD 500 nm
5.00 kV 3.0 100000x TLD 4.0

558

559

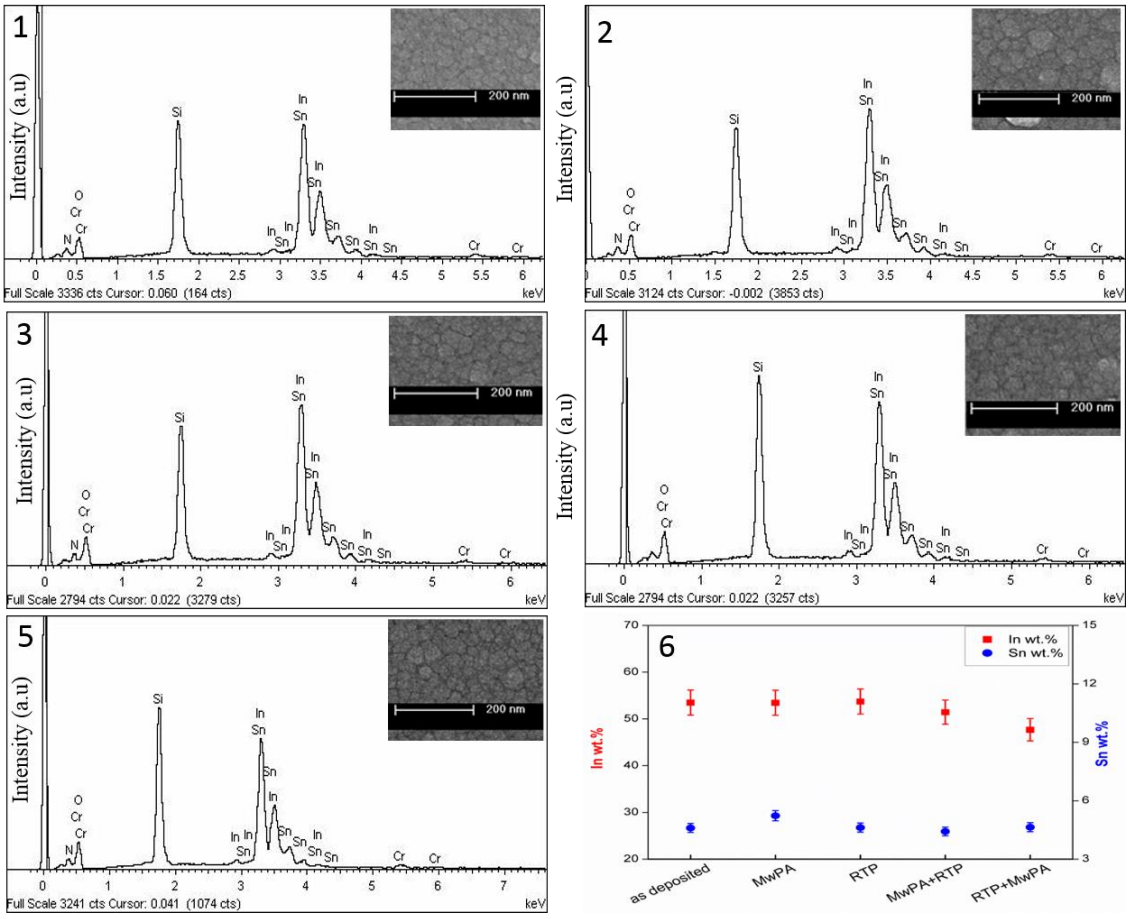

560

561

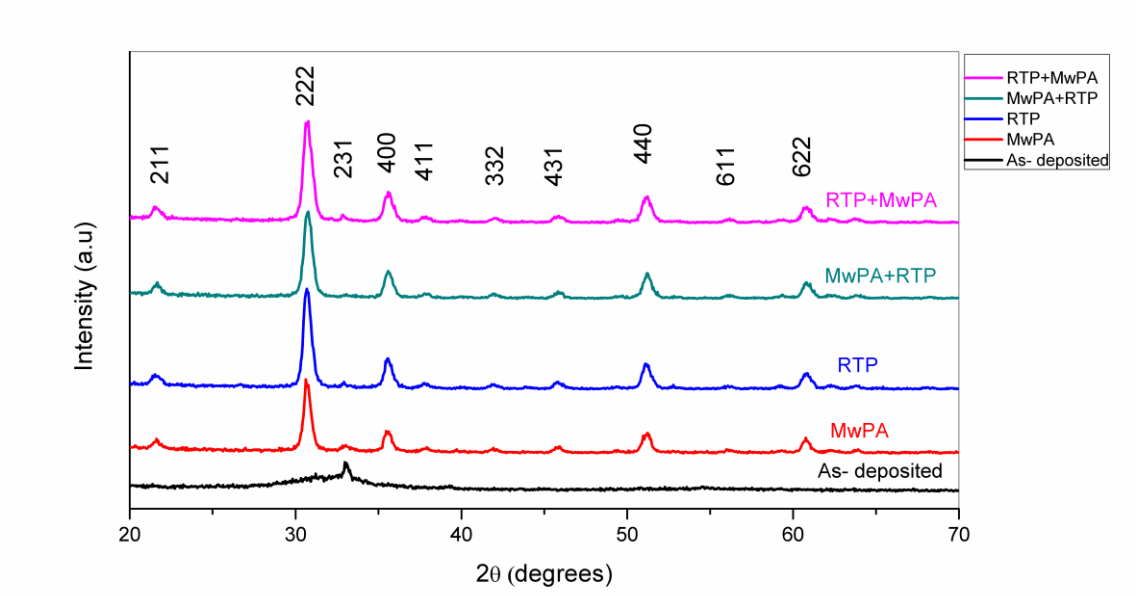

562

563

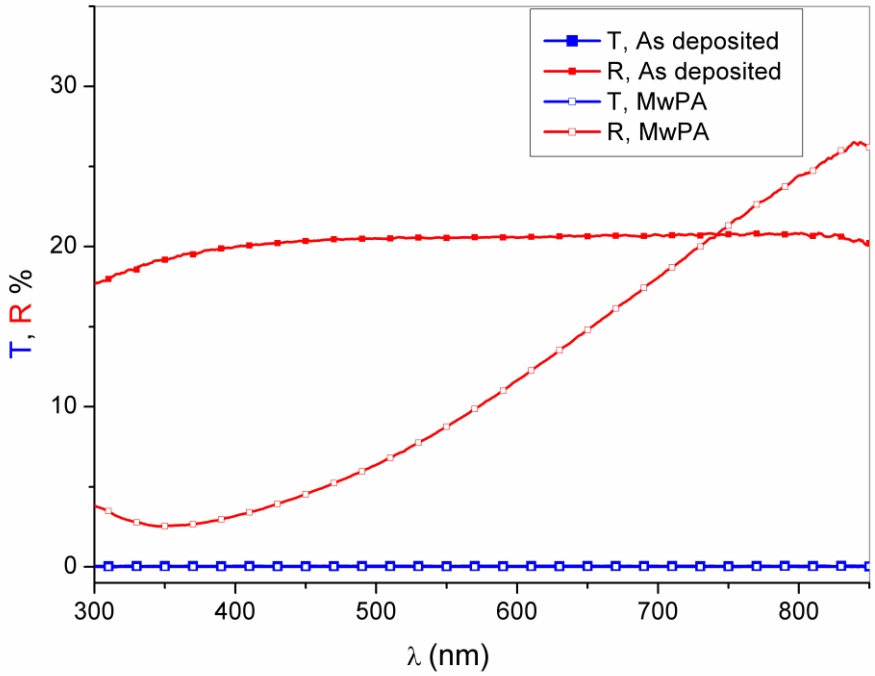

564

565

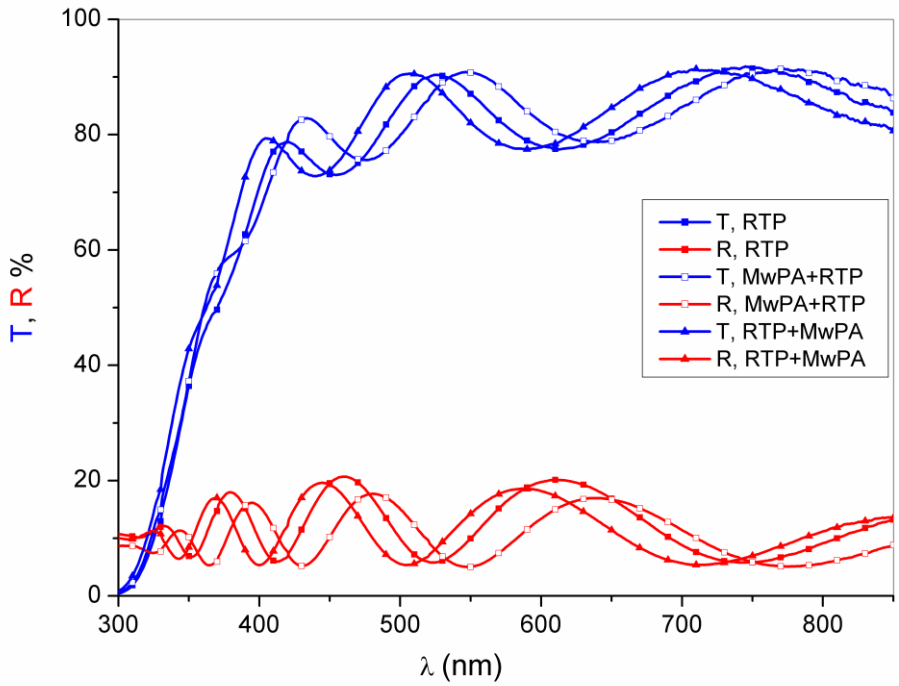

566

567

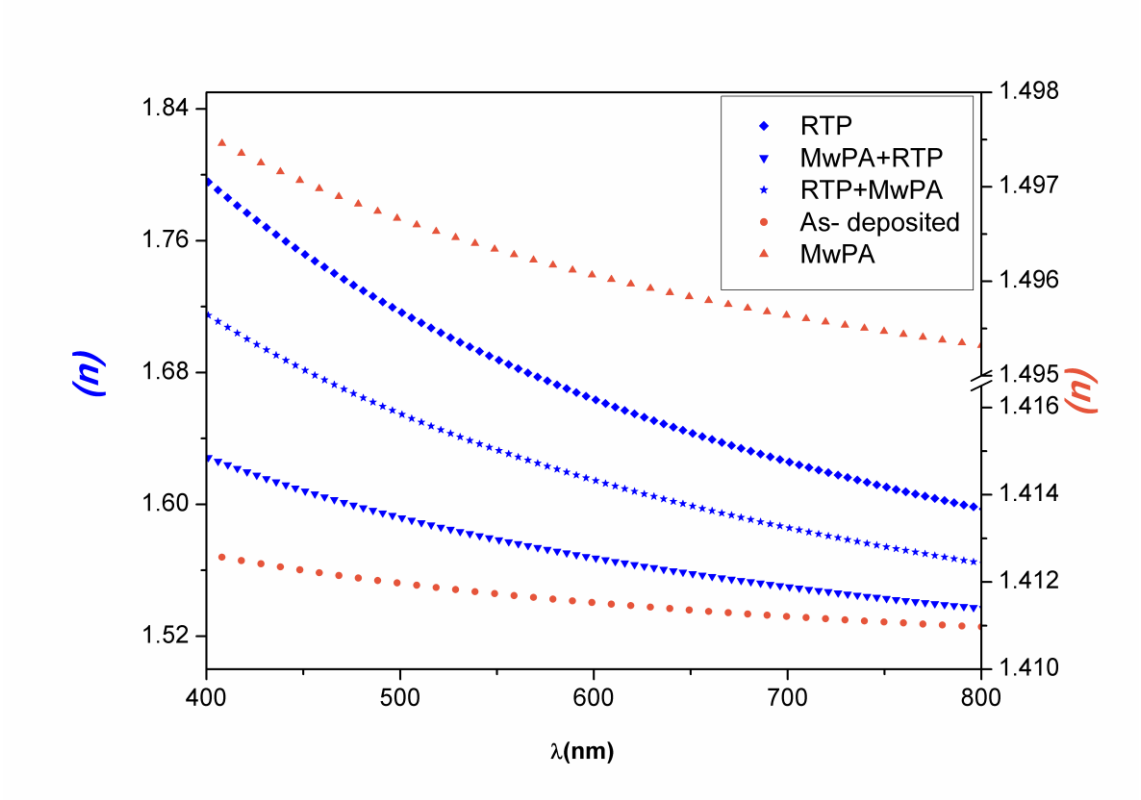

568

569

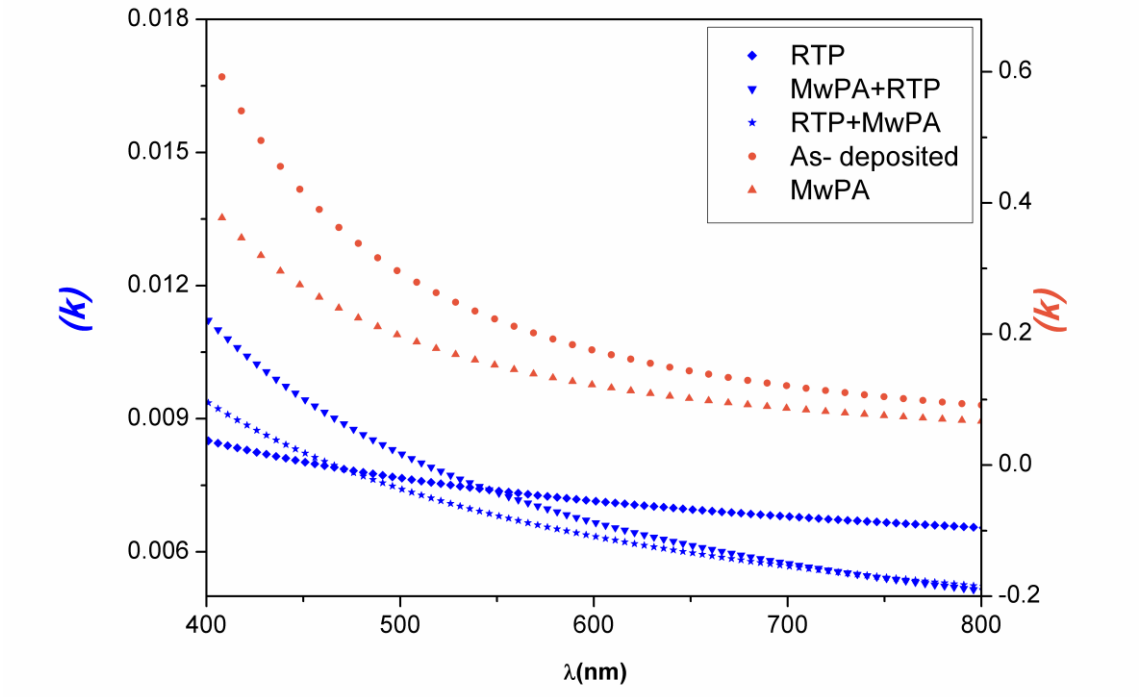

570

571

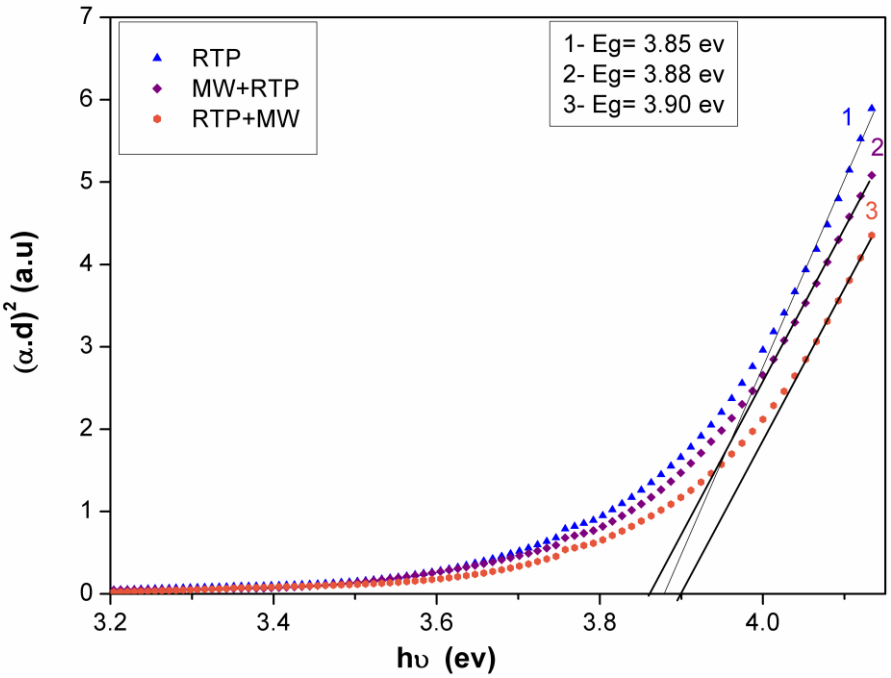

572

573

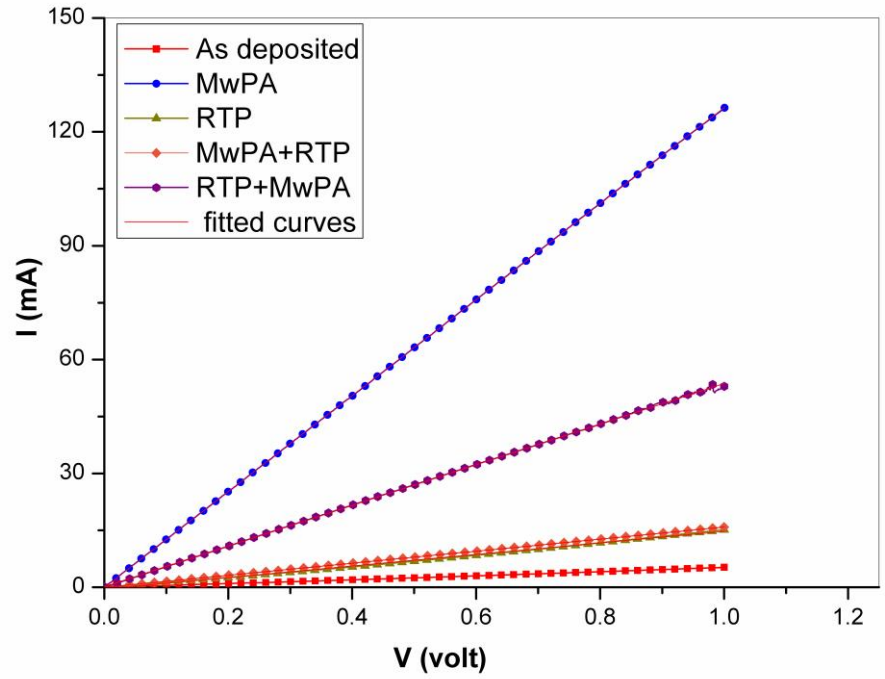

574

575

576

577